JOURNAL OF MATERIALS SCIENCE 31 (1996) 4149–4157

Effects of nondensifying inclusions on the densification and microstructure of zinc oxide matrix composites

TOSHIO KIMURA*, HIDETO KAJIYAMA‡, RYUICHI YAZAKI§, TAKASHI YAMAGUCHI
Faculty of Science and Technology, Keio University, Yokohama 223, Japan

The densification and microstructure development of ZnO containing $Zn_7Sb_2O_{12}$, ZrO_2, and aggregated ZnO were investigated to elucidate the effect of nondensifying inclusions on the sintering of ceramic/ceramic composites. The inclusion retarded the densification, and the degree of retardation was found to depend on the chemical species of inclusion; $Zn_7Sb_2O_{12}$ had the largest effect, followed by ZrO_2 and then aggregated ZnO last. The experimental results for aggregated ZnO was explained by the theory which predicts the generation of backstresses. The backstresses give a less significant effect on the densification. For $Zn_7Sb_2O_{12}$ and ZrO_2, the microstructure of the matrix varied with distance from an inclusion particle; much porosity was observed in the region surrounding the inclusion. Circumferential voids, which are responsible for the suppression of densification, form during the initial stage of sintering. Inclusion particles generate an anchoring effect which retards the densification of the matrix immediately surrounding the inclusion particle during the intermediate stage.

1. Introduction

Structural heterogeneities such as agglomerates, non-uniform particle packing, and solid second-phase particles reduce the densification rate of green compacts of crystalline ceramic materials. The agglomerates and non-uniform particle packing can be eliminated by improving processing methods. The solid second-phase particles (inclusions), however, are essential for ceramic/ceramic composites. Nondensifying inclusions reduce the densification rate and cause defects in the microstructure. Hot pressing and hot isostatic pressing are used for the fabrication of ceramic/ceramic composites to increase sintering rate and reduce such defects. It is worth investigating the densification behaviour and microstructure development during sintering of composites under ambient pressure, not only to improve the properties of sintered composites but also to better understand the sintering phenomenon.

The effect of inclusions on sintering has been studied both theoretically [1–9] and experimentally [9–32]. Fan and Rahaman [30] summarized the explanation proposed to account for the reduction in the densification rate of a compact containing nondensifying inclusions; (i) generation of the large viscoelastic backstress within the matrix [2, 3, 6, 7], (ii) rigid, contiguous network formation by the inclusions [5, 9, 29–31], (iii) crack-like void formation in the matrix [12, 29], (iv) differential sintering caused by non-uniform packing of the matrix particles [22, 30, 31], (v) an anisotropic stress state [7], and (vi) coarsening of the matrix particles [7]. No single explanation can account for all of the experimental results reported in the literature [9–32]. More experimental evidence is necessary to elucidate the effect of inclusions during sintering.

This paper is an extension of our previous work [23], in which the densification behaviour of ZnO containing $Zn_7Sb_2O_{12}$ particles was examined. In this work we used three species for inclusions; $Zn_7Sb_2O_{12}$, ZrO_2, and aggregated ZnO. These materials do not react with ZnO and neither new chemical compounds nor liquid phase form at the temperatures examined [23, 30–34]. However, different physical interaction such as adhesion is expected. The effect of inclusions was examined from densification behaviour and microstructure development during constant-rate heating and isothermal heating experiments. The degree of suppression of densification was found to be dependent on the chemical species of the inclusions;

*Supported by the Inamori Foundation.
‡Present address: Sony Corp., Atsugi, Kanagawa 243, Japan.
§Present address: Nippon Sanso Corp., Kitakoma-gun, Yamanashi 408 Japan.

0022–2461

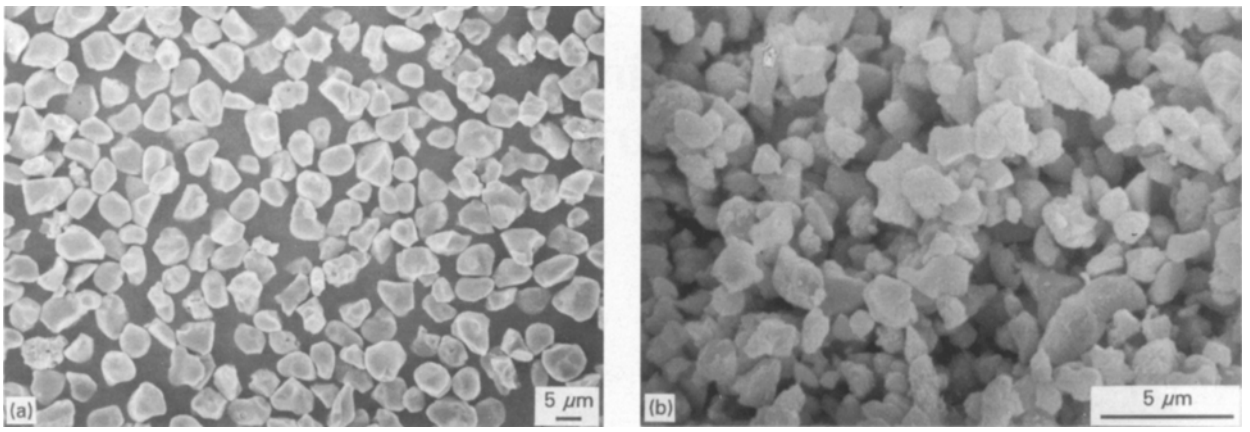

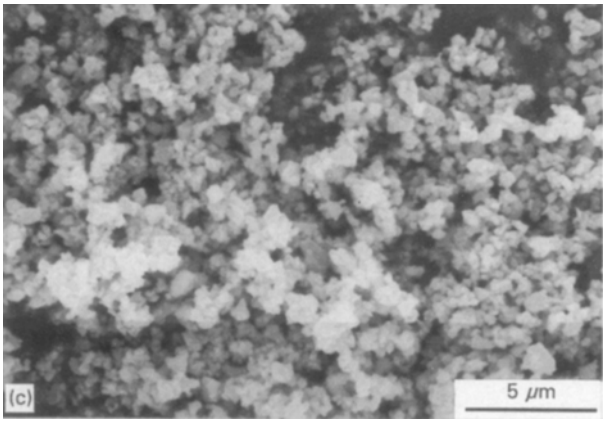

Figure 1 SEM photographs of (a) coarse, (b) medium, and (c) fine $Zn_7Sb_2O_{12}$ powders.

the effect of $Zn_7Sb_2O_{12}$ was the largest and that of aggregated ZnO was the smallest.

2. Experimental procedure

The preparation method of $Zn_7Sb_2O_{12}$ powders is described in our previous paper [23]. ZrO_2 powders were prepared as follows. As-received ZrO_2 powder (average particle size was about 0.9 μm: Daiichi Kigenso Kagaku Kogyo Co., Ltd., Tokyo, Japan) was pressed at 98 MPa. The resultant compact was divided into small pieces, and then heated at 1400 °C for 5 h. The product was ground with an SiC mortar and classified by sedimentation in water into two groups (1 to 3 and 6 to 10 μm). The powder with a particle size of < 1 μm was prepared by the same method described above, except for the pressing procedure; the loose powder was heated. The aggregated ZnO powders were made by a similar method: as-received ZnO loose powder (Seido Chemical Co., Ltd., Osaka, Japan), which was used as a matrix powder, was heated at 1100 °C for 1.5 h, ground with an agate mortar, and classified into two groups (1 to 3 and 6 to 10 μm). We will refer to powders with particle size < 1, 1 to 3, and 6 to 10 μm as fine, medium, and coarse, respectively. Fig. 1 shows the SEM photographs of $Zn_7Sb_2O_{12}$ powders and Table I shows the median particle sizes determined by the sedimentation method (Model CAPA-500, Horiba Ltd., Tokyo, Japan). Fig. 1 indicates that the particle size distribution is sharp. The other powders had a similar appearance except for the coarse aggregated ZnO, in which the surface of the particle was not smooth and pores were observed.

A zinc oxide powder with an average particle size of about 0.7 μm was mixed with the inclusion powders in a ball mill for 20 h. The reduction in particle size during ball milling was less significant, because a plastic bottle and balls lined with plastic were used. Ethanol was used as a medium. After drying at 80 °C, the mixture was pressed into discs 11.3 mm in diameter and 3 mm thick. The compacting pressure was changed for each sample (between 35 and 55 MPa) to obtain a constant density for the ZnO matrix (54% of theoretical). The compacts were heated at a constant rate of 5 °C min^{-1} from room temperature up to 1300 °C in a dilatometer (Model DL-1500, Shinku-Riko, Tokyo, Japan) or at constant temperatures. The sample was inserted into a furnace and kept at a constant temperature for isothermal heating. The true densities of 5.78, 6.20, and 5.825 g cm^{-3} for ZnO, $Zn_7Sb_2O_{12}$, and ZrO_2, respectively, were used to calculate relative density and volume fraction of the inclusions. The microstructure was observed by scanning electron microscopy (SEM; Model T-20, JEOL, Tokyo, Japan) on polished sections, which were etched thermally or chemically using a 1% $HClO_4$–ethanol solution. Some compacts were polished after the impregnation of sulfur [35]. Fracture surfaces were observed for samples with low densities.

TABLE I Particle size of powders used as inclusion

	Particle size (μm)		
	$Zn_7Sb_2O_{12}$	ZrO_2	ZnO
Coarse	6.89	5.50	5.60
Medium	1.58	1.32	1.80
Fine	0.75	0.70	

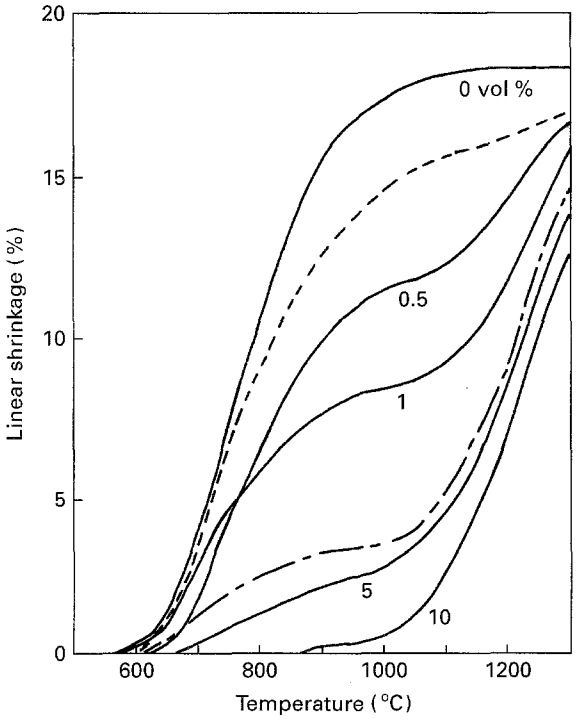

Figure 2 Shrinkage curves during constant-rate heating of ZnO containing various amounts of medium $Zn_7Sb_2O_{12}$. (– – –) and (— · —) curves are for ZnO containing 1 vol % coarse and fine $Zn_7Sb_2O_{12}$, respectively.

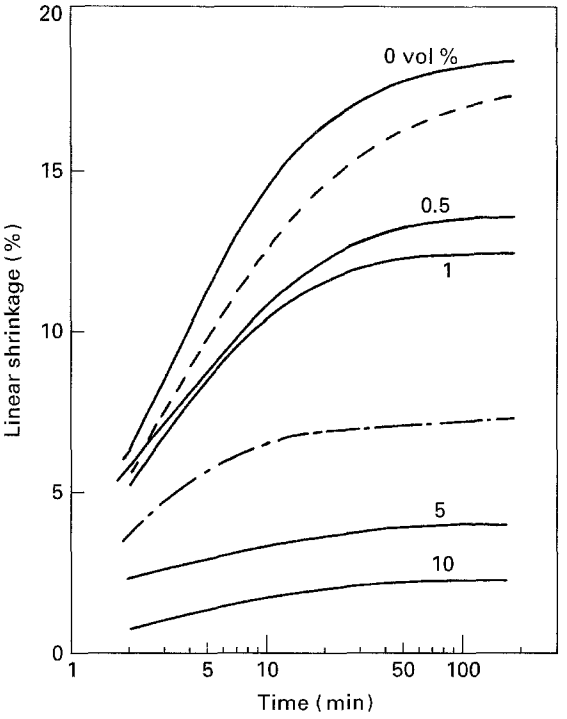

Figure 3 Isothermal shrinkage at 900 °C for ZnO containing various amounts of medium $Zn_7Sb_2O_{12}$. (– – –) and (— · —) curves are for ZnO containing 1 vol % coarse and fine $Zn_7Sb_2O_{12}$, respectively.

3. Results

3.1. $Zn_7Sb_2O_{12}$

Fig. 2 shows the effect of $Zn_7Sb_2O_{12}$ volume fraction and particle size on the shrinkage curves during constant-rate heating. The shrinkage curves for other volume fractions and particle sizes are illustrated in our previous paper [23]. The effect of $Zn_7Sb_2O_{12}$ particles on densification are summarized as follows. (i) An increase in volume fraction and a decrease in particle size of $Zn_7Sb_2O_{12}$ increases the degree of retardation of the densification. (ii) Two-step densification behaviour is observed for some samples. The former is also reported in a ZnO–SiC system [20].

Fig. 3 shows the isothermal shrinkage curves at 900 °C. As observed in the constant-rate heating experiments, the densification rate decreased with an increase in volume fraction and with a decrease in particle size. The densification rate decreased after 40 min.

Fig. 4 shows the microstructures of compacts containing 1 vol % medium size $Zn_7Sb_2O_{12}$ particles, withdrawn from the furnace at 800 and 900 °C during constant-rate heating. Voids developed at the inclusion–matrix interface during the initial stage of sintering. We will refer to this void as a circumferential void.

Fig. 5 shows the microstructure of compacts containing 1 vol % coarse $Zn_7Sb_2O_{12}$ particles, heated isothermally at various temperatures for 1 h. These photomicrographs were taken for the compacts at the final stage of sintering; the densities of these compacts were almost constant at 95%. In the 900 °C sample (Fig. 4a), the region in the immediate vicinity of the inclusion particles is dark, indicating higher porosity than in the matrix. On the

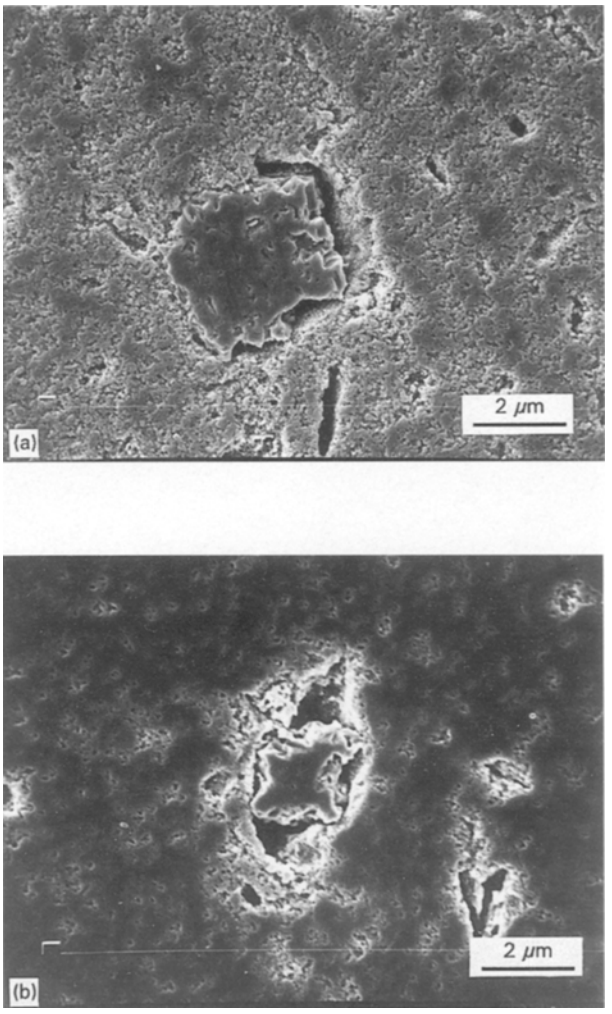

Figure 4 Microstructures of ZnO–medium $Zn_7Sb_2O_{12}$ (1 vol %) composites withdrawn at (a) 800 and (b) 900 °C during constant-rate heating. The densities were (a) 65.6 and (b) 69.7%.

other hand, in 1000 and 1100 °C samples pores are accumulated at the boundary between the inclusion and the matrix. At 1200 °C, a part of the inclusion surface is in contact with the matrix, but large pores are found adjacent to the inclusion particles.

Fig. 6 shows the microstructure of compacts containing 5 vol % coarse $Zn_7Sb_2O_{12}$ particles, fired at 1000 and 1100 °C. The rate of pore removal was large in the matrix away from the inclusions. Pore accumulation at the inclusion–matrix interface observed above 1000 °C in Fig. 5 does not occur up to 1100 °C, because the overall densification rate is dependent on the volume fraction of inclusions and the microstructure is closely related to the density.

Fig. 7 shows the microstructure change for a sample with heavily suppressed densification. The large particles in Fig. 7a are $Zn_7Sb_2O_{12}$ and the smaller ones are ZnO. Heating at 900 °C for 1 h hardly increased the density. Increasing the temperature increased density slightly, but the most noticeable characteristic is the coarsening of the ZnO particles. Grain coarsening is probably caused by surface diffusion or evaporation–condensation.

The microstructure observations revealed that suppression of densification occurred mainly in the matrix near the inclusion particles. The shrinkage of samples heated at 900 °C for 3 h is plotted against the surface area of inclusions per unit volume, equivalent

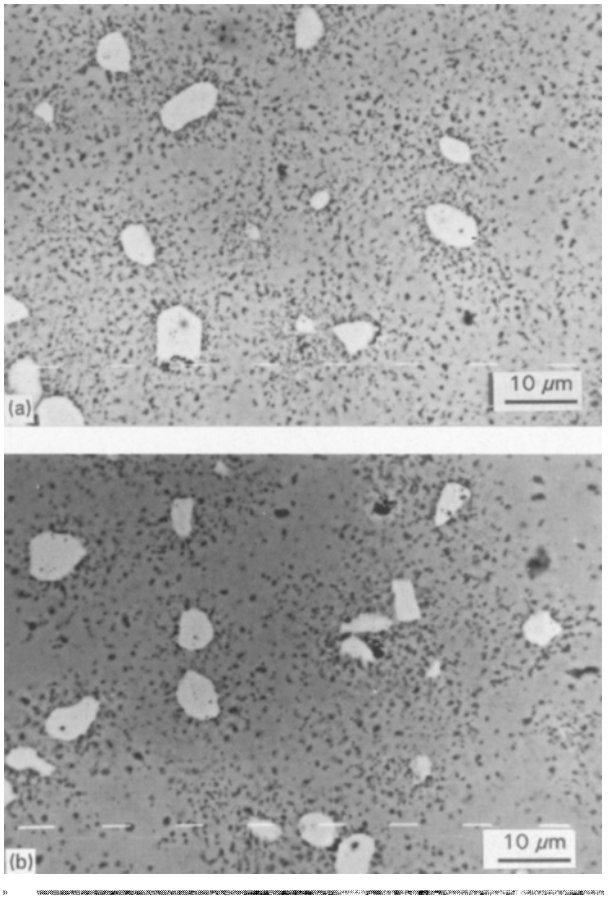

Figure 6 Microstructures of ZnO–coarse $Zn_7Sb_2O_{12}$ (5 vol %) composites fired at (a) 1000 and (b) 1100 °C for 1 h. The densities were (a) 89.9 and (b) 91.8%.

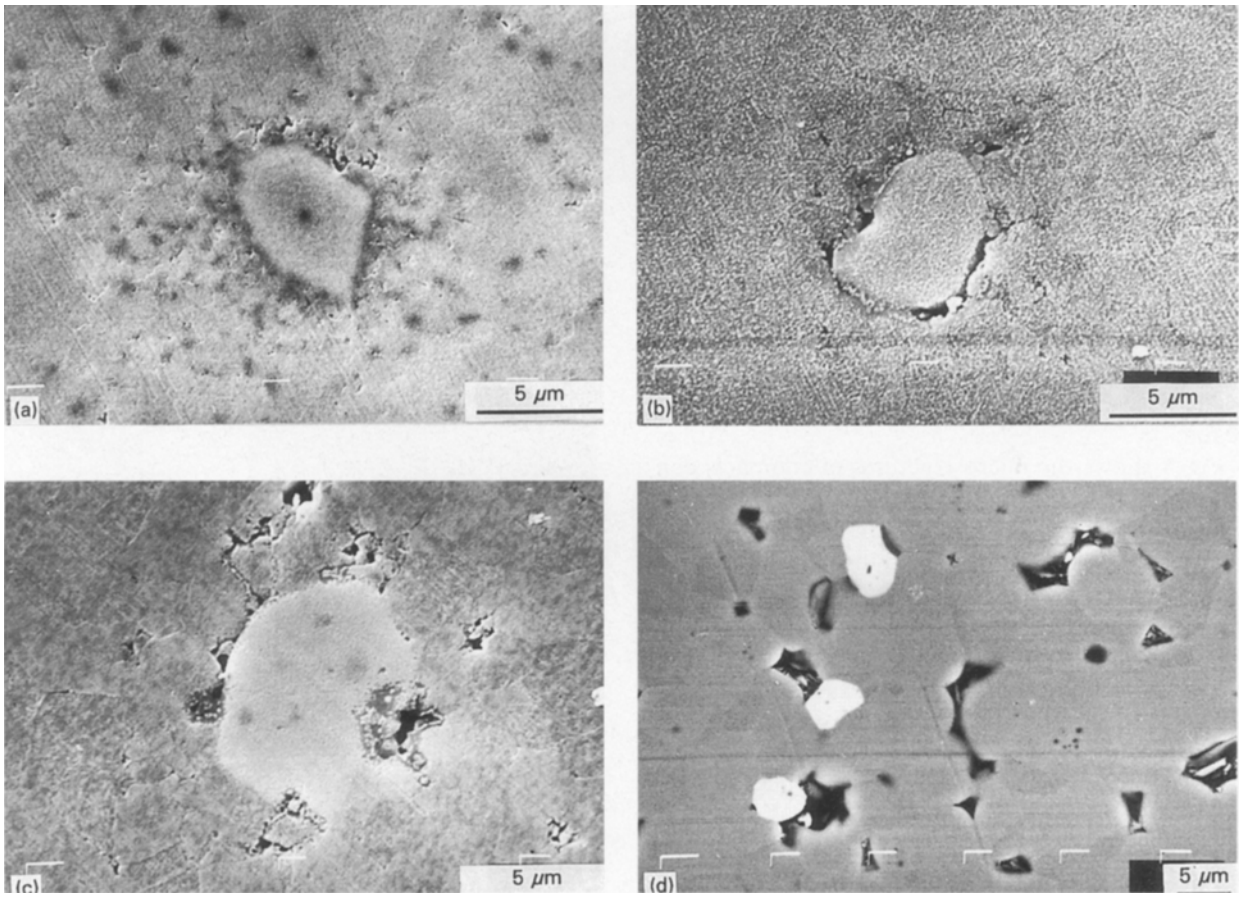

Figure 5 Microstructures of ZnO–coarse $Zn_7Sb_2O_{12}$ (1 vol %) composites fired at (a) 900, (b) 1000, (c) 1100, and (d) 1200 °C for 1 h. The densities were (a) 92.5, (b) 95.6, (c) 95.3, and (d) 95.2%.

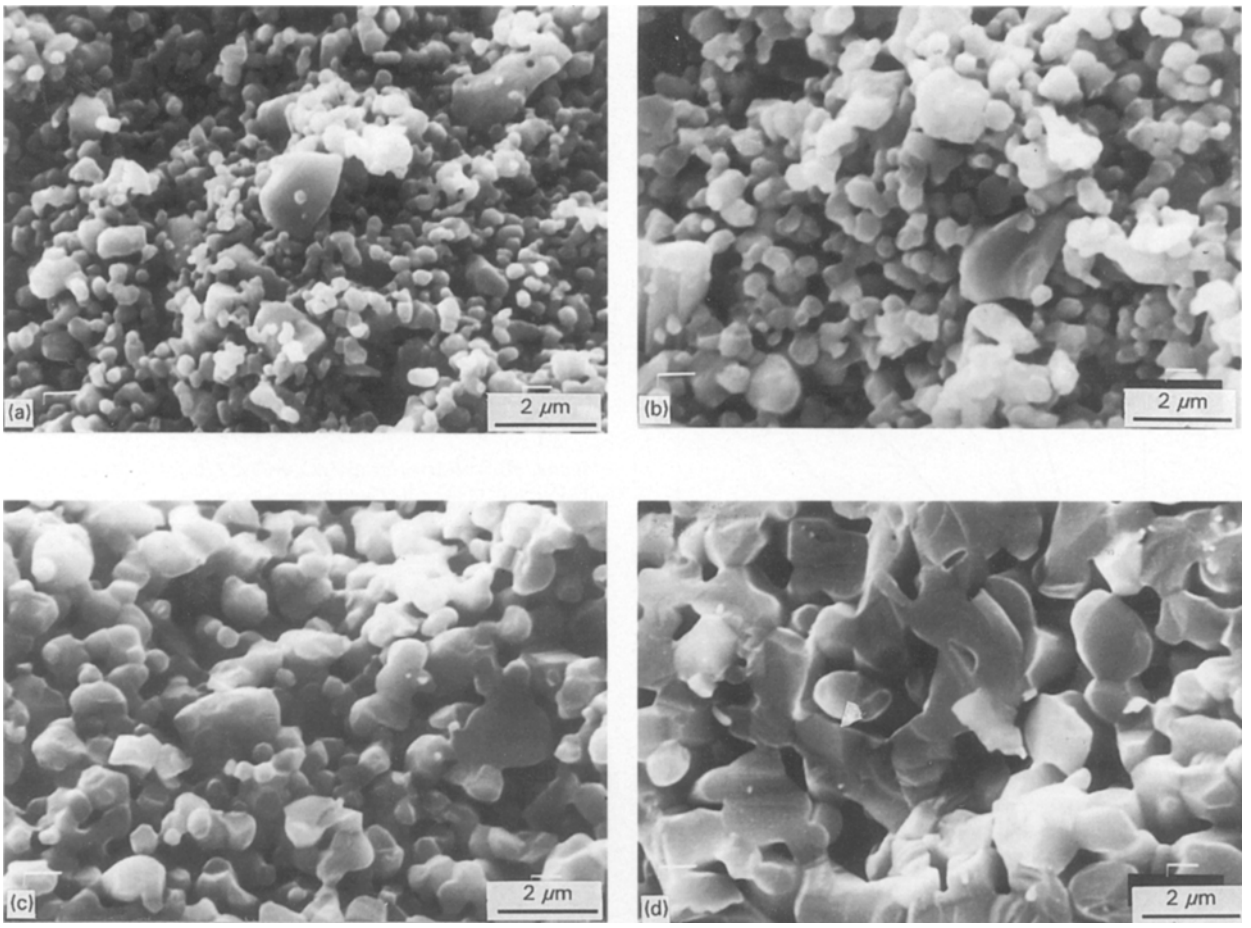

Figure 7 SEM photographs of fracture surfaces of ZnO-medium $Zn_7Sb_2O_{12}$ (10 vol%) composites fired at (a) 900, (b) 1000, (c) 1100, and (d) 1200 °C for 1 h. The densities were (a) 57.4, (b) 63.2, (c) 70.7, and (d) 85.1%.

to the boundary area between the inclusions and the matrix (Fig.8, circles). A close correlation is observed. The relation between the shrinkage and the number of inclusion particles in unit volume gave a poor correlation. The result shown in Fig. 8 indicates that the densification of the matrix near an inclusion is suppressed, which is consistent with the microstructural observation. An increase in volume fraction of inclusions with the same particle size and a decrease in inclusion size with the same volume fraction both increase the boundary area between the matrix and the inclusion, resulting in the suppression of densification to a large extent.

3.2. ZrO_2

Fig. 9 shows the effect of ZrO_2 volume fraction and particle size on the shrinkage curve for the constant-rate heating experiment. In this case also, an increase in ZrO_2 volume fraction and a decrease in particle size increased the degree of suppression on densification. In no case, however, was two-step densification behaviour observed. Isothermal densification at 900 °C was also retarded. The relation between the shrinkage of the samples and the surface area of the inclusion particles in unit volume is shown in Fig. 8 (squares). A close correlation is observed as in the $Zn_7Sb_2O_{12}$ case, but with different magnitudes of densification retardation; ZrO_2 is less effective in suppressing the densification.

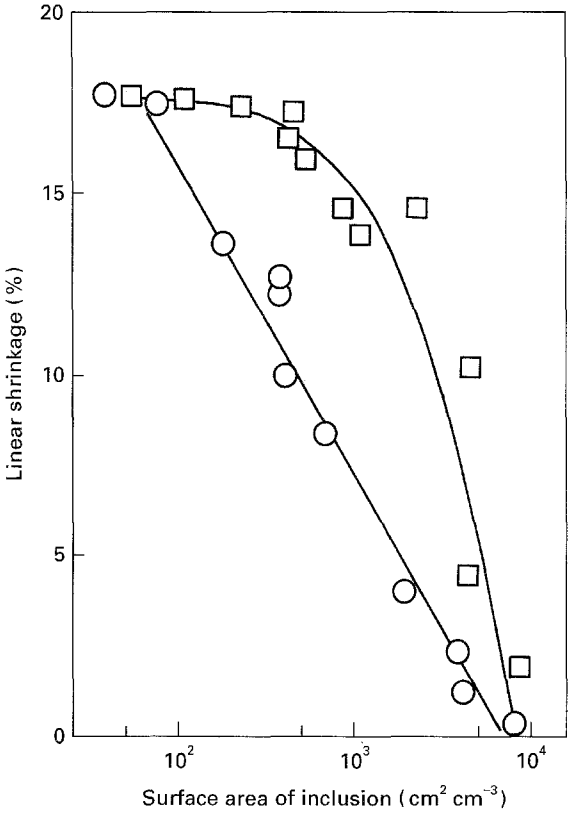

Figure 8 Effect of surface area of inclusions per unit volume on linear shrinkage of composites containing (○) $Zn_7Sb_2O_{12}$ and (□) ZrO_2 fired at 900 °C for 3 h.

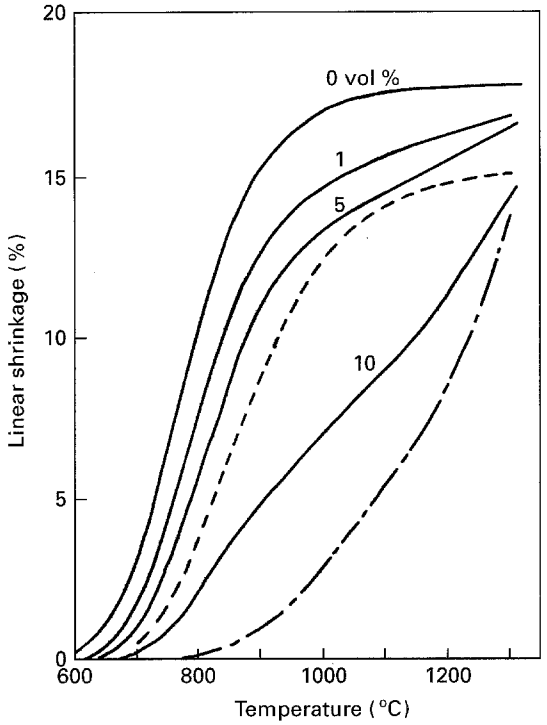

Figure 9 Shrinkage curves during constant-rate heating of ZnO containing various amounts of medium ZrO_2. (– – –) and (— · —) curves are for ZnO containing 10 vol % coarse and fine ZrO_2, respectively.

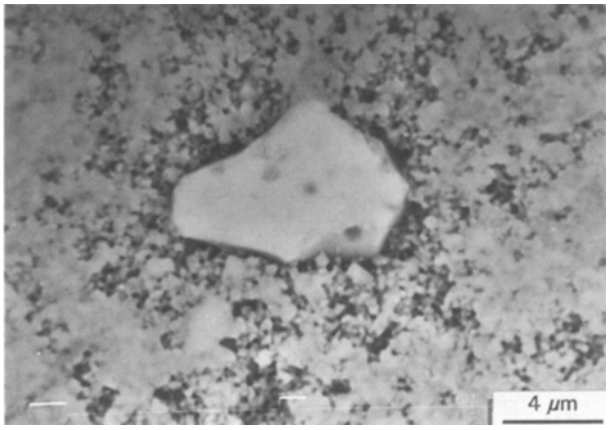

Figure 10 Microstructure of ZnO–coarse ZrO_2 (5 vol %) composite fired at 900 °C for 3 min. The density was 72.2%.

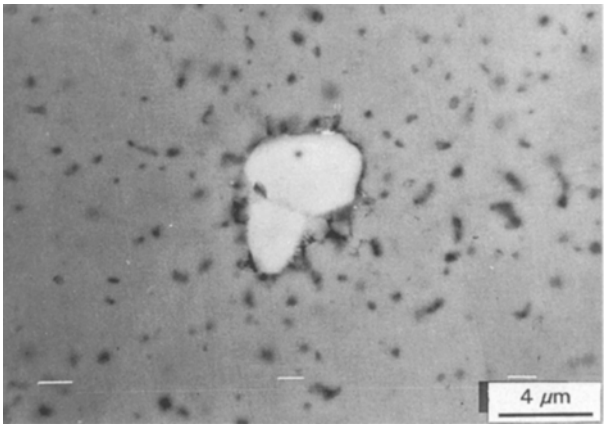

Figure 11 Microstructure of ZnO–coarse ZrO_2 (1 vol %) composite fired at 900 °C for 1 h. The density was 94.2%.

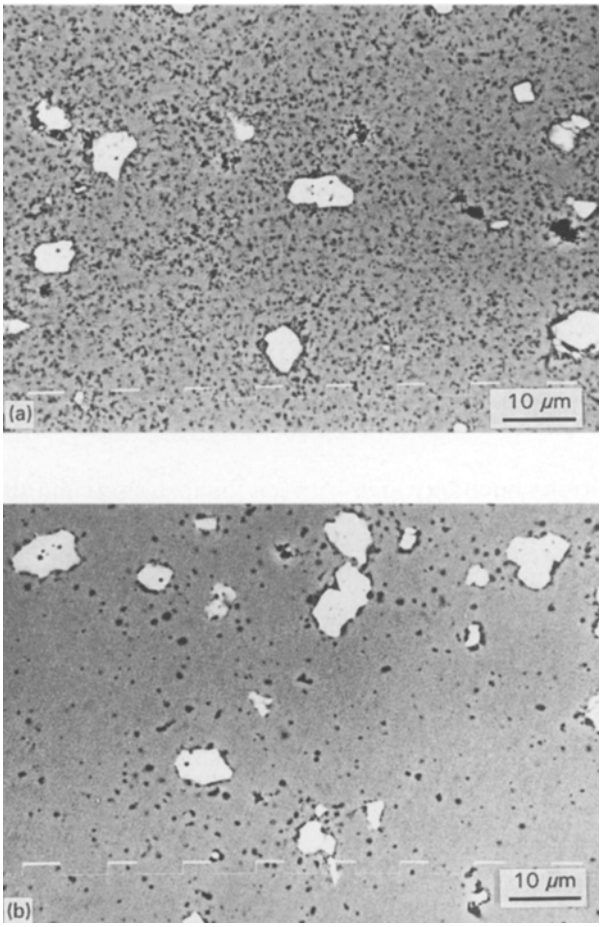

Figure 12 Microstructures of ZnO–coarse ZrO_2 (5 vol %) composites fired at (a) 900 and (b) 1000 °C for 1 h. The densities were (a) 88.5 and (b) 94.8%.

Fig. 10 shows the microstructure of a sample containing 5 vol % of coarse ZrO_2 particles heated at 900 °C for 3 min (the density was 72.2%). A circumferential void formed in this system. Fig. 11 shows the microstructure of a sample containing 1 vol % of coarse ZrO_2 particles heated at 900 °C for 1 h. Comparison of Fig. 11 with Fig. 5a and b indicates that the porosity around the inclusion is smaller for ZrO_2 than for $Zn_7Sb_2O_{12}$.

Fig. 12 shows the microstructures of samples containing 5 vol % coarse ZrO_2 heated at 900 and 1000 °C. Comparison of Fig. 12 with Fig. 6 reveals the different densification behaviour between the samples containing ZrO_2 and $Zn_7Sb_2O_{12}$. The densities were both about 89% for the two samples shown in Figs 12a and 6a. The porosity in the matrix away from the inclusions was smaller for $Zn_7Sb_2O_{12}$ than ZrO_2, indicating extensive pore accumulation around $Zn_7Sb_2O_{12}$. An increase in the heating temperature by 100 °C reversed the situation (Figs 12b and 6b). The porosity in the matrix was smaller for ZrO_2 than for $Zn_7Sb_2O_{12}$, and most pores were located near the ZrO_2 particles. Pores in the matrix were eliminated faster than those around inclusions. These microstructural differences explain why ZrO_2 had a smaller effect on the densification suppression. Inclusion particles

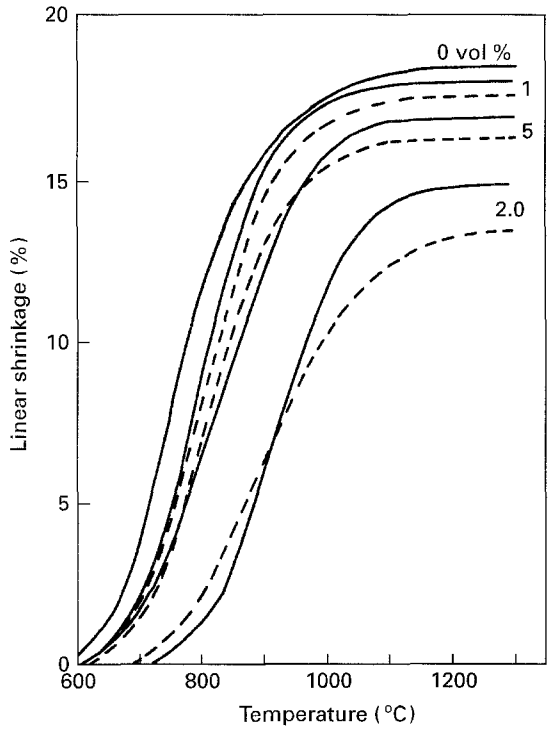

Figure 13 Shrinkage curves during constant-rate heating of ZnO containing various amounts of (——) medium and (– – –) coarse aggregated ZnO.

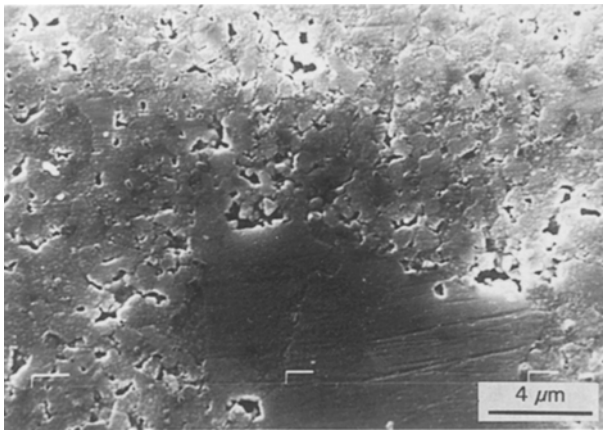

Figure 14 Microstructure of ZnO containing 5 vol % large aggregated ZnO fired at 800 °C for 3 h.

reduced the densification rate of the matrix immediately surrounding an inclusion. The region in the matrix influenced by the inclusions is smaller for ZrO_2 than for $Zn_7Sb_2O_{12}$. Thus, the result shown in Fig. 8 is obtained.

3.3. Aggregated ZnO

Fig. 13 shows the shrinkage curves for the constant-heating rate experiments of ZnO containing various amounts of aggregated ZnO with different particle sizes. An increase in the volume fraction of aggregated ZnO decreased the densification rate, but the effect of particle size was not so obvious. Comparison of Fig. 13 with Figs 2 and 9 indicates that aggregated ZnO has the smallest effect in retarding densification.

The distinction between the matrix and inclusion particles in the microstructure was difficult, because they had the same chemical composition and the aggregated ZnO particles were also polycrystalline. However, there was no indication of the presence of circumferential voids in the cross-section of samples. 5 vol % of large aggregated ZnO particles (10 to 44 μm) were added to ZnO and heated at 800 °C for 3 h to observe the microstructure (Fig. 14). Large pores, like those observed in the samples containing $Zn_7Sb_2O_{12}$ and ZrO_2, were not observed for this sample, and necks were developed between the inclusion and matrix particles.

4. Discussion

The experimental results are summarized as follows:

1. The addition of nondensifying inclusions reduces the densification rate. The degree of reduction is dependent on the chemical species of inclusions.
2. For $Zn_7Sb_2O_{12}$ and ZrO_2, the reduction in densification rate is not homogeneous throughout the matrix. The circumferential voids form during the initial stage, and the densification of the matrix just around inclusions is heavily suppressed during all the stages of sintering.
3. The reduction in densification rate is closely related to the surface area of inclusion particles for $Zn_7Sb_2O_{12}$ and ZrO_2.

The theoretical analysis [2, 3, 6] based on the generation of backstresses can explain the experimental results for aggregated ZnO, because the calculated maximum stresses are smaller than the sintering stresses for a system with a positive Poisson's ratio [6, 7]. The aggregated ZnO inclusions had a small effect on the reduction of densification. Furthermore, the inclusion particle size had a less significant effect (Fig. 13), as predicted by the theory [2, 3, 6]. Stearns *et al.* [28] also reported no effect of nondensifying $YBa_2Cu_3O_{6+x}$ inclusions on the densification of $YBa_2Cu_3O_{6+x}$ matrix. This result agrees with our ZnO inclusions–ZnO matrix experiment.

For $Zn_7Sb_2O_{12}$ and ZrO_2, another explanation is necessary. One possible explanation of the large suppression of densification by $Zn_7Sb_2O_{12}$ and ZrO_2 is the chemical reaction between the inclusion and the matrix. However, the circumferential void formed during the initial stage breaks the contact between the inclusion and the matrix. A chemical reaction is not possible under these circumstances. Thus, the chemical reaction is ruled out as an explanation for the large suppression of densification.

The circumferential voids (Figs 4 and 10 for the $Zn_7Sb_2O_{12}$ and ZrO_2 inclusions, respectively) are responsible for the large suppression of densification during the initial stage. A circumferential void forms when the inclusion particle sinters faster than the matrix [2], but this is not the case for the present system. For our systems, the degree of adhesion between inclusion and matrix will determine whether a circumferential void forms or not. The adhesion is

physical in nature or chemical by neck formation. When the degree of adhesion is large, as in the case for aggregated ZnO, the inclusion and matrix are mechanically continuous, and radial compressional and hoop tensile stresses develop by the densification of the matrix [2, 3, 6, 7], and no circumferential voids form. For $Zn_7Sb_2O_{12}$ and ZrO_2, the degree of adhesion at the initial stage is small, and the inclusion–matrix interface acts as the incipient separation plane [26]. We will consider a small volume element of matrix just surrounding an inclusion. The densification of the matrix puts tensile stresses on this volume element. The stress parallel to the inclusion–matrix interface is symmetrical, whereas that perpendicular to the interface is asymmetrical. The densification of the matrix moves this volume element away from the interface, resulting in the formation of a circumferential void.

The densification during the intermediate stage (i.e. the densification of the second step for the $Zn_7Sb_2O_{12}$-containing samples above 900 °C) occurs by the densification of the matrix around the inclusions. Figs 4 and 9 indicate that the inclusion particle is not completely separated from the matrix by the circumferential void. There are some contact points between the inclusion and the matrix. These contact points give an anchoring effect on the densification of the matrix immediately surrounding the circumferential void. The densification of the matrix parallel to the circumferential void is suppressed by the anchoring effect. The magnitude of the anchoring effect in the matrix is a function of the distance from the inclusion–matrix interface; the effect is largest just around the circumferential void. The matrix is divided into two regions. Region I locates near inclusions, and the densification rate is reduced in this region. Region II is the matrix away from the inclusions.

During the constant-rate heating experiment, region II densifies at low temperatures (between 600 and 900 °C, which is the temperature range for the densification of pure ZnO). The densification of region I occurs at high temperatures (above 900 °C). The volume of region I in a green compact determines the shrinkage of the compact at this stage, where the densification of region II finishes. The shrinkage at this stage is nearly equal to that achieved by heating compacts containing $Zn_7Sb_2O_{12}$ and ZrO_2 at 900 °C for 3 h. The volume of region I is proportional to the product of the thickness of region I and the surface area of the inclusions. Thus, the inclusion surface area is closely related to the degree of reduction in densification rate as illustrated in Fig. 8. The thickness of region I is larger for $Zn_7Sb_2O_{12}$ than for ZrO_2, probably because ZnO adheres to ZrO_2 more than to $Zn_7Sb_2O_{12}$.

A $Zn_7Sb_2O_{12}$ inclusion heavily suppresses the densification of region I, resulting in the separation of the temperature ranges of densification of regions I and II. Hence, the two-step densification curve during constant-rate heating results. For ZrO_2, the temperature ranges overlap, resulting in the single-step densification curve.

Two processes occur during heating the samples above 900 °C; one is the densification of region I, which results in the densification of the compact, and the other is the formation of large pores. The densification of region II is almost completed at the stage when the densification of region I starts. Creep in the densified region II permits the reduction in volume of region I, resulting in the densification of the compact. The sintered region II, however, prevents full densification of region I. Thus, pores remain and the density of sintered region I is lower than that of sintered region II. Pores coalesce during the final stage of sintering, resulting in the large pores in the matrix just around inclusions.

When the volume fraction of the inclusions is small, region II is continuous and region I is separated by the region II matrix. An increase in the volume fraction of inclusions increases the volume of region I, and finally region I becomes continuous and region II is isolated. In this case, the densification of the compact occurs over the temperature range at which region I densifies (above 900 °C). Thus, a single-step densification curve results during constant-rate heating (10 vol% in Fig. 2). Particle coarsening by surface diffusion and/or evaporation–condensation, which is responsible for the microstructure development shown in Fig. 7, also occurs, because the densification occurs at high temperatures.

5. Conclusions

The densification behaviour of ceramic/ceramic composites is determined by the degree of adhesion between the inclusion and the matrix. When the degree of adhesion is large, the difference in densification rates generates a compressive stress in the inclusion and also backstresses in the matrix. These backstresses are less significant for the densification. Thus, aggregated ZnO gave a small effect on the densification of ZnO–aggregated ZnO composites. When the degree of adhesion is small, a circumferential void forms around an inclusion particle during the initial stage, resulting in the suppression of densification during the initial stage. The anchoring effect of inclusions suppresses the densification of the matrix during the intermediate stage. The magnitude of this effect is a function of distance from the inclusion–matrix interface. The densification of matrix around inclusions (region I) is suppressed, whereas that of the matrix away from an inclusion (region II) is hardly affected by the inclusions. Region II densifies between 600 and 900 °C, which is the temperature range for the densification of pure ZnO. Region I densifies above 900 °C. $Zn_7Sb_2O_{12}$ retards the densification greatly in region I, resulting in the two-step densification curves during constant-rate heating. The temperature ranges, over which regions I and II densify, overlap for ZnO containing ZrO_2, resulting in the single-step densification curves.

References

1. A. G. EVANS, *J. Amer. Ceram. Soc.* **65** (1982) 497.
2. R. RAJ and R. K. BORDIA, *Acta Metall.* **32** (1984) 1003.

3. C. H. HSUEH, A. G. EVANS, R. M. CANNON and R. J. BROOK, *ibid.* **34** (1986) 927.
4. C. H. HSUEH, *J. Mater. Sci.* **21** (1986) 2067.
5. F. F. LANGE, *J. Mater. Res.* **2** (1987) 59.
6. G. W. SCHERER, *J. Amer. Ceram. Soc.* **70** (1987) 719.
7. R. K. BORDIA and G. W. SCHERER, *Acta Metall.* **36** (1988) 2411.
8. S. SUNDARESAN and I. A. AKSAY, *J. Amer. Ceram. Soc.* **73** (1990) 54.
9. O. SUDRE, B. BAO, B. FAN, F. F. LANGE and A. G. EVANS, *ibid.* **75** (1992) 525.
10. K. D. REEVE, *Amer. Ceram. Soc. Bull.* **42** (1963) 452.
11. W. H. RHODES, *ibid.* **64** (1981) 19.
12. F. F. LANGE and M. METCALF, *ibid.* **66** (1983) 389.
13. B. KELLETT and F. F. LANGE, *ibid.* **67** (1984) 369.
14. R. K. BORDIA and R. RAJ, in Proceedings of the Twenty-first University Conference on Ceramic Science, University Park, PA, July 1985 (Materials Science and Research, Vol. 20), edited by R. E. Tressler, G. L. Messing, C. G. Pantano and R. E. Newnham (Plenum, New York, 1986) p. 27.
15. R. K. BORDIA and R. RAJ, *J. Amer. Ceram. Soc.* **69** (1986) C-55.
16. L. C. DE JONGHE, M. N. RAHAMAN and C. H. HSUEH, *Acta Metall.* **34** (1986) 1467.
17. M. N. RAHAMAN and L. C. DE JONGHE, *J. Amer. Ceram. Soc.* **70** (1987) C-348.
18. C. P. OSTERTAG, *ibid.* **70** (1987) C-355.
19. R. K. BORDIA and R. RAJ, *Adv. Ceram. Mater.* **3** (1988) 122.
20. M. W. WEISER and L. C. DE JONGHE, *J. Amer. Ceram. Soc.* **71** (1988) C-125.
21. R. K. BORDIA and R. RAJ, *ibid.* **71** (1988) 302.
22. L. C. DE JONGHE and M. N. RAHAMAN, in Proceedings of the Materials Research Society, San Diego, CA, April 1989, edited by I. A. Aksay, G. L. McVay and D. R. Ulrich (Materials Research Society, Pittsburgh, PA, 1989) p. 353.
23. T. KIMURA, H. KAJIYAMA, J. KIM and T. YAMAGUCHI, *J. Amer. Ceram. Soc.* **72** (1989) 140.
24. W. H. TUAN, E. GILBART and R. J. BROOK, *J. Mater. Sci.* **23** (1989) 1062.
25. W. H. TUAN and R. J. BROOK, *ibid.* **24** (1989) 1953.
26. F. F. LANGE, *Acta Metall.* **37** (1989) 697.
27. M. N. RAHAMAN and L. C. DE JONGHE, *J. Amer. Ceram. Soc.* **73** (1990) 602.
28. L. C. STEARNS, M. P. HARMER and H. M. CHAN, *ibid.* **73** (1990) 2740.
29. O. SUDRE and F. F. LANGE, *ibid.* **75** (1992) 519.
30. C.-F. FAN and M. N. RAHAMAN, *ibid.* **75** (1992) 2056.
31. *Idem, ibid.* **75** (1992) 2066.
32. O. SUDRE and F. F. LANGE, *ibid.* **75** (1992) 3241.
33. J. KIM, T. KIMURA and T. YAMAGUCHI, *J. Mater. Sci.* **24** (1989) 213.
34. T. SENDA and R. C. BRADT, *J. Amer. Ceram. Soc.* **74** (1991) 1296.
35. C. GRESKOVICH and K. W. LAY, *ibid.* **55** (1972) 142.

Received 7 March 1994
and accepted 1 December 1995